Structural, calorimetric, and Monte Carlo investigation of the order-disorder transition of BF_4 in $(CH_3)_4NBF_4$

E. Palacios, J. J. Melero, and R. Burriel
Instituto de Ciencia de Materiales de Aragón, Consejo Superior de Investigaciones Científicas and Universidad de Zaragoza, 50009 Zaragoza, Spain

P. Ferloni
Dipartimento di Chimica Fisica and CSTE-CNR, Università di Pavia, 27100 Pavia, Italy
(Received 21 February 1996)

The structural and thermodynamic properties of $(CH_3)_4NBF_4$ have been studied with single-crystal x-ray diffraction and heat-capacity measurements. The low-temperature space group symmetry $P42_1m$ has been determined, with cell parameters $a=11.556(2)$ Å, $c=5.718(1)$ Å, $V=763.6(2)$ Å^3, and $Z=4$, at 120 K. At 200 K, the structure is $P4/nmm$ and the cell parameters $a=8.204(2)$ Å, $c=5.798(2)$ Å, $V=390.2(2)$ Å^3, and $Z=2$. The heat-capacity data showed a λ anomaly at 158.1 ± 0.1 K, with entropy content $\Delta S=R\ln 4$, corresponding to the structural phase transition. This transition is produced by a cooperative low-temperature ordering of the BF_4 tetrahedra on a single arrangement from a high-temperature statistical disorder among four orientations. The heat-capacity anomaly has been analyzed in terms of Landau theory and the critical exponents have been determined. Monte Carlo simulations based on octupole-octupole electrostatic interactions in planes perpendicular to the c direction provide the same type of ordering and a similar transition temperature. [S0163-1829(96)01337-9]

I. INTRODUCTION

Several tetrasubstituted alkyl-ammonium salts with general formula R_4NBF_4, where R may range from the methyl to the n-hexyl group, are commonly used in electrochemistry as supporting electrolytes in aqueous and nonaqueous solutions. However, their properties in the solid state have not been researched much until now.

A previous differential scanning calorimetry (DSC) study[1] showed the existence of phase transitions or weak thermal anomalies in the first four members of the family, from R = methyl to n-buthyl. In the case of $(CH_3)_4NBF_4$, a transition was reported at $T_0 = 154\pm1$ K, with an anomalous enthalpy content $\Delta H\approx0.5\pm0.1$ kJ/mol, which was initially ascribed to the onset of isotropic rotations of the $(CH_3)_4N$ groups.[2] This kind of process is usual among tetramethylammonium compounds, such as the nitrate, chlorate, perchlorate, and the halides,[3] all of which seem to undergo phase transitions between 120 K and 250 K due to reorientations of the methyl and the tetramethyl groups.

Measurements of NMR relaxation times[4] on $(CH_3)_4NBF_4$ revealed an activation energy $E_a = 23.4$ kJ/mol for the thermally activated motion of the $(CH_3)_4N^+$ ion and a dramatic increase of the boron relaxation rate at 150 K, explained as a possible order-disorder transition involving the F^- ions.

The room-temperature (RT) crystal structure of $(CH_3)_4NBF_4$ (Ref. 5) is tetragonal, $P4/nmm$, with $a=8.231$ Å, $c=5.889$ Å, and $Z=2$, where the BF_4 groups are located with one B-F bond lying on the fourfold axis, and the other F^- ions making a triangle in a disordered distribution among several possible random orientations. The center of the $(CH_3)_4N$ group lies on a 4 axis parallel to the tetragonal fourfold axis and the group is orientationally ordered. So an ordering of the BF_4 groups is expected below RT.

The compounds $(CH_3)_4NXO_4$ (X = Cl, I, Mn, and Re) are isostructural with $(CH_3)_4NBF_4$ however, their low-temperature structures are not known. All of them are constituted by two blocks of essentially tetrahedral groups and each one is known to produce structural transitions in different compounds. It is interesting to know which of them plays a role in the low-temperature ordering, carrying out a thorough investigation of the structural transition of the tetrafluoroborate as a model compound for a variety of similar isostructural salts with the same cation and different anions.

The octupole-octupole interaction is responsible for the ordering in many solid compounds with molecular groups, NH_4Cl (Ref. 6), NH_4AlF_4 (Ref. 7), or CH_4 (Ref. 8) being among the best studied cases. Since the octupolar moment of BF_4 is considerably larger than those of NH_4 or CH_4, one would expect a complete orientational order up to room temperature. This type of interaction has been studied in large tetrahedral groups like SO_4, SeO_4, ClO_4, and BeF_4.[9]

The octupolar interaction decreases rapidly with distance and can approximately be confined to the nearest neighbors. Moreover, depending on the relative orientation of the octupoles, the interaction can be strongly directional dependent; from a practically cubic spatial arrangement one can obtain almost purely two-dimensional interactions. It is also interesting to analyze the possibility of long-range order in two dimensions with this interaction. Additionally, strong interaction energies can surprisingly produce cooperative effects at much lower temperatures, sometimes of a different order of magnitude. The study of the electrostatic interactions in $(CH_3)_4NBF_4$ can illustrate some of these unexpected phenomena.

 © 1996 The American Physical Society

In this work we aimed at determining the type of structural transition of $(CH_3)_4NBF_4$ by solving the low-temperature (LT) structure and studying the relation with the RT phase. The thermodynamic parameters of the transition have been calculated from heat-capacity measurements. The molecular origin of the structural change has also been analyzed in terms of the electrostatic interactions of the BF_4 groups. The thermal evolution has been followed with Monte Carlo simulations and compared with the structural and calorimetric results.

The paper has been organized as follows: Section II reports the determination of the structures of $(CH_3)_4NBF_4$ at 120 K and 200 K, below and above the transition temperature, by single-crystal x-ray diffraction. The equilibrium orientations of the BF_4 groups have been characterized. The lattice parameters have been followed with powder diffraction patterns between 100 K and 300 K. Section III describes the heat-capacity measurements between 5 K and 350 K in an adiabatic calorimeter. In Sec. IV the lattice contribution has been estimated from the different degrees of freedom in this structure and the anomalous contribution of the transition has been analyzed with Landau theory. Section V explains the electrostatic calculations to obtain the different interaction energies for all the possible orientations of the four nearest neighbors of each BF_4. Monte Carlo simulations of this system are used to obtain the equilibrium configuration at each temperature and the thermodynamic functions through the order-disorder transition. The final conclusions are given in Sec. VI.

II. X-RAY DIFFRACTION

Transparent crystals of prismatic shape were obtained by recrystallization from an aqueous solution of commercial Fluka purum $(CH_3)_4NBF_4$ in bidistilled water. Rotation photographs of several crystals were taken at 300 K with a polaroid camera. All of them showed broad reflections and the best crystal was chosen for the intensity collection.

The LT structure was determined from the intensities of the Bragg reflections, at 120 K, in a four-circle Siemens diffractometer, with Mo $K\alpha$ radiation ($\lambda = 0.710\,73$ Å). A nitrogen jet Cryostream cooler was used as the cryogenic system. The temperature was maintained within ± 1 K. After proper orientation of the crystal, rotation photographs around the a, b, and c axes, at 120 K, were consistent with a tetragonal unit cell with $a \approx 11.56$ Å and $c \approx 5.72$ Å (i.e., approximately $a = \sqrt{2}a_0$, $c = c_0$; a_0 and c_0 being the cell parameters at RT,[5] with doubling of the cell volume). A data collection of 25 strong reflections was made in order to obtain the orientation matrix. Some of them had a wide or asymmetric profile, but a better crystal was not available. A collection of 2909 reflections, $0 < \theta < 30°$, $-10 \leqslant h \leqslant 16$, $0 \leqslant k \leqslant 16$, and $0 \leqslant l \leqslant 8$, was scanned.

The refinement of the orientation matrix gave the cell parameters $a = 11.556(2)$ Å, $c = 5.718(1)$ Å, $V = 763.6(2)$ Å^3, and $Z = 4$. The systematic absences were $h00$, $h = 2n+1$, and $0k0$, $k = 2n+1$, produced by two 2_1 axes parallel to a and b, respectively. Two space groups are compatible with these absences, $P42_1m$ and $P42_12$, with an internal consistency index $R = 0.085$ for 1398 unique reflections. The group $P42_1m$ was chosen because $P42_12$ is a subgroup of $P4/nmm$ with $a = a_0$, not with $a = \sqrt{2}a_0$. Then, this symmetry would imply a complex reconstructive transition, very improbable considering the calorimetric data, which are typical of a continuous or quasicontinuous transition. Moreover, the $P42_12$ group maintains the fourfold axis, discarding the BF_4 ordering. By inspection of the common symmetry elements of the RT and LT groups, one can assign the $\bar{4}$ axis and the 2 axis to the c axes through the center of each type of $(CH_3)_4N^+$ ions. Tentatively, the B atom was placed at the same site it occupies in the room-temperature phase, after proper transformation of coordinates. In the foregoing calculations the SHELX program[10] was used. Successive Fourier difference syntheses gave the position of the F and C atoms, reaching $R = 0.19$ with equal weights, $w = 1$. In the next step, anisotropic thermal factors were introduced, reaching $R = 0.12$. The Fourier difference finally gave the position of the hydrogen atoms, labeled H1–H4 in Table I and Fig. 1. The remaining H5, H6, and H7 were refined starting on the positions deduced from the pyramidal geometry of the CH_3 groups. Because of the rather poor internal consistency of reflections, 81 parameters were refined in the last stages and only the 699 unique reflections with $I > 10\sigma$ were considered, using equal weights and resulting $R = 0.073$. Table I shows the list of the final structural parameters and standard deviations, while some distances and angles are shown in Table II. Structure factor tables have been deposited.[11] Using a weight $w = 1/(\sigma^2 + 0.1F^2)$ yielded to $R = 0.078$ and $R_w = 0.096$. The use of 900 unique reflections with $I > 5\sigma$ raised R to 0.094 with no significant changes in the atomic coordinates. The final Fourier difference showed maxima of $0.75e/$Å^3 in the plane of F21 and F22, in points corresponding to other orientations of the BF_4, being probably an indication of some remaining orientational disorder of these groups.

The structure of the LT phase (see Fig. 1) can be described as deriving from the RT phase when the BF_4 molecules chose, in an ordered way, one of the four equivalent orientations, resulting an antiferro-ordered structure of four sublattices. Some slight changes occurred in the other atomic coordinates, the most significant one being an 8° rotation of the $(CH_3)_4N$ groups centered in N1 around the [001] direction, approaching H1, H3, and H7 to the nearest F21. It should be noted that the ordering may produce four type of domains, depending on the orientation chosen by each particular BF_4 and its neighbors. However, the four types of domains are crystallographically related either by a (1/2,1/2,0) translation or by inversion with respect to an inversion center of the $P4/nmm$ space group, and give practically the same diffraction pattern. Thus, there are two kind of indistinguishable domains (except when they coexist at both sides of a domain wall) and two other ones related with the first set by an inversion center.

At RT, the powder diffraction diagram was taken with a rotating anode in a D-max Rigaku diffractometer with Cu $K\alpha$ radiation, 2θ varying from 6° to 80° with steps of 0.02°. The diffractogram agreed basically with the structure described in Fig. 1, with an additional disorder of the BF_4 groups. There is a slight difference with respect to the previously reported structure[5] that describes one B-F bond along the fourfold axis of the structure and the other three F^- ions

TABLE I. Fractional atomic coordinates and thermal parameters at 120 K. Standard deviations in parenthesis. The U_{ij} values are given in units of 10^{-3} Å^2. Isotropic thermal factors are used for hydrogen atoms.

Atom	Site	x/a	y/b	z/c	U_{11}	U_{22}	U_{33}	U_{12}	U_{13}	U_{23}
N1	2*b*	0	0	1/2	57(5)	U_{11}	10(5)	0	0	0
N2	2*c*	1/2	0	0.5127(12)	5(2)	U_{11}	12(4)	−2(3)	0	0
F1	4*e*	0.2514(3)	0.7514(3)	0.1670(5)	37(1)	U_{11}	17(1)	−3(4)	2(1)	U_{13}
B	4*e*	0.2594(5)	0.7594(5)	0.9257(9)	24(2)	U_{11}	15(2)	−6(5)	−1(2)	U_{13}
F21	8*f*	0.1320(3)	0.2318(4)	0.1427(6)	68(2)	73(3)	46(2)	−45(2)	35(2)	−15(2)
F22	4*e*	0.1814(4)	0.6814(4)	0.8295(11)	161(5)	U_{11}	38(4)	−122(5)	−16(2)	U_{13}
C1	4*e*	0.0771(6)	0.5771(6)	0.3346(18)	44(3)	U_{11}	36(5)	2(5)	28(3)	U_{13}
C2	8*f*	0.0819(6)	0.9383(6)	0.3499(13)	23(3)	26(3)	20(3)	−3(2)	−10(2)	0(2)
C3	4*e*	0.4218(5)	0.9218(5)	0.3619(18)	28(3)	U_{11}	29(4)	−13(3)	−12(2)	U_{13}
H1	8*f*	0.362(4)	0.548(4)	0.245(7)	8(8)					
H2	8*f*	0.012(5)	0.632(6)	0.240(8)	40(11)					
H3	8*f*	0.389(4)	0.640(4)	0.472(6)	2(8)					
H4	8*f*	0.374(6)	0.988(5)	0.271(8)	39(10)					
H5	4*e*	0.120(5)	0.620(5)	0.393(10)	52(12)					
H6	4*e*	0.373(5)	0.873(5)	0.408(10)	65(12)					
H7	8*f*	0.484(6)	0.647(6)	0.241(9)	62(11)					

(two of them labeled as F21 and one as F22 in this work) distributed in 24 positions on a plane perpendicular to it, with some disorder in the position of the mass center of BF_4. On the contrary, the profile analysis of the powder diffractogram gave a better refinement assuming one B-F bond (B-F1 in this work) in the fourfold axis and the other three distributed in 12 positions with equal probability. The thermal parameters for these atoms are so large (U = 0.1 Å^2), one can say that F21 and F22 are quasi-isotropically distributed over a circle around the B-F1 axis. This interpretation is practically equivalent to the one given in Ref. 5.

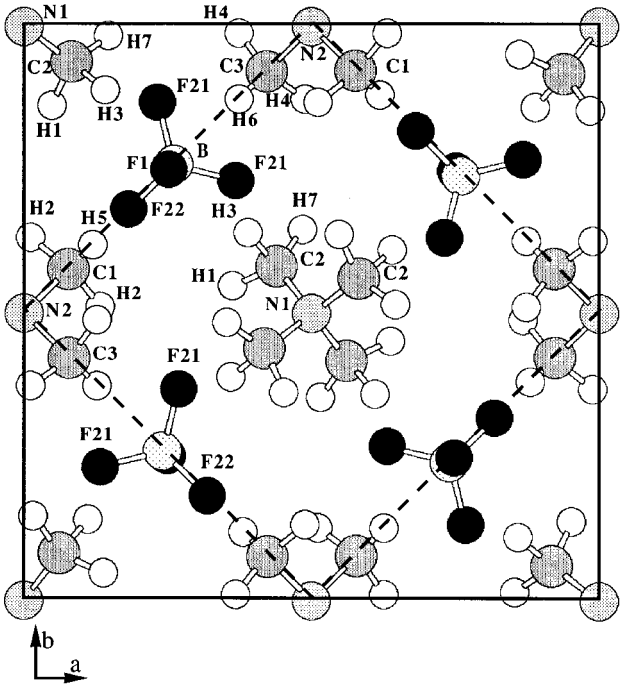

FIG. 1. Projection of the low-temperature structure of $(CH_3)_4NBF_4$ on the ab plane. In the high-temperature phase, the orientations of the BF_4 groups are randomly distributed among the four orientations obtained by successive 90° rotations around the B-F axis perpendicular to the drawing.

In order to clarify this ambiguity, a short collection of 684 reflections, with 217 unique reflections, was taken at 200 K, where the thermal motions should have a smaller amplitude than at 300 K. The resulting space group is $P4/nmm$, like at 300 K, and the lattice parameters $a=8.204(2)$ Å, $c=5.798(2)$ Å, $V=390.2(2)$ Å^3, and Z = 2. The refining procedure started with the structural parameters proposed in Ref. 5. The last steps were carried out with 41 fitting parameters with equal weight for every reflection. The successive least squares cycles converged to the values given in Table III. Structure factor tables have been deposited.[11] The final reliability index $R=0.063$ is good for a crystal of this quality, and the internal consistency index, averaging over the

TABLE II. Selected interatomic distances and angles for the structure at 120 K, with their standard deviations.

Distance (Å)		Angle (deg)	
N1-C1	1.464(7)	C2(i)-N1-C2(ii) [a]	110(1)
		C2(i)-N1-C2(iii) [a]	108(1)
N2-C1	1.534(9)	C1-N2-C1	111(1)
N2-C3	1.542(8)	C3-N2-C3	112(1)
		C1-N2-C3	109(1)
B-F1	1.386(6)	F1-B-F21	109(1)
B-F21	1.353(7)	F1-B-F22	108(1)
B-F22	1.388(8)	F21-B-F21	111(1)
		F21-B-F22	109(1)
C1-H2	1.12(6)	N2-C1-H2	102(5)
C1-H5	0.8(1)	N2-C1-H5	119(8)
C2-H1	1.13(4)	N1-C2-H1	117(5)
C2-H3	1.12(4)	N1-C2-H3	105(4)
C2-H7	1.11(6)	N1-C2-H7	122(8)
C3-H4	1.07(6)	N2-C3-H4	99(5)
C3-H6	0.8(1)	N2-C3-H6	127(9)

[a]Symmetry codes: (i) $x,1-y,z$; (ii) $y-1,x,1-z$; (iii) $\overline{x},y-1,z$.

TABLE III. Fractional atomic coordinates and thermal parameters at 200 K. Standard deviations in parentheses. The $\langle U \rangle$ values are given in units of 10^{-3} Å^2. Isotropic thermal factors are used for hydrogen atoms.

Atom	Site	x/a	y/b	z/c	$\langle U \rangle$ [a]
N	2*b*	3/4	1/4	1/2	30(10)
B	2*c*	1/4	1/4	0.921(3)	37(5)
F1	8*i*	0.256(11)	1/4	0.156(1)	57(7)
F21	16*k*	0.149(2)	0.387(2)	0.865(2)	80(10)
F22	8*i*	0.382(2)	1/4	0.825(4)	100(10)
C	8*i*	1/4	0.560(1)	0.350(1)	47(3)
H1	8*i*	1/4	0.506(5)	0.476(7)	91(10)
H2	16*k*	0.355(4)	0.596(4)	0.253(6)	91(9)

[a] $\langle U \rangle = \frac{1}{3}(U_{11}+U_{22}+U_{33})$.

equivalent reflections, is $R=0.07$. The structure is similar to the one found at 300 K, as described in Ref. 5, but F22 lies in the $8i$ mirror plane positions $(1/4,y,z)$ and equivalent ones; the two F21 atoms are mutually symmetric with respect to this plane. Therefore, the F22 atoms are distributed among four positions around the B-F1 axis, and the eight corresponding F21 positions are determined by the rigid tetrahedral structure of the BF_4 group. It means that the BF_4 group can occupy anyone of the four distinguishable orientations, at random. There is not any other structural transition between 200 K and RT.

Powder diffractograms have been taken from 100 K to 300 K with Guinier geometry and Cu $K\alpha_1$ radiation. Figure 2 shows the evolution of the cell constants with temperature (for the LT phase $a/\sqrt{2}$ is plotted). The absence of any anomaly around 158 K indicates a negligible coupling between the order parameter and the lattice strains.[12] Superstructure reflections corresponding to the LT phase are observed below 158 K. A slight shift of the cell constants determined from powder diffraction with respect to the values from the single crystal must be due to a small error in the origin of θ. It is not important because the powder diffraction experiments were intended to scan the evolution of a and c with T. The process was not optimized for obtaining good absolute values.

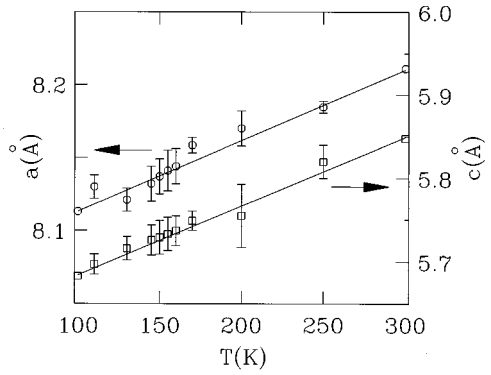

FIG. 2. Variation of the cell constants with temperature, calculated from powder diffraction experiments. For the LT phase $a/\sqrt{2}$ has been plotted instead of a. The straight lines are guides to the eye.

III. HEAT CAPACITY: EXPERIMENT

A collection of about 50 crystals with a total mass of 1.0047 g was used for the heat-capacity experiments. The sample was placed in a copper vessel of 1 ml sealed with 70 torr of helium gas inside to improve the heat exchange and reduce the thermal equilibration times. The sample vessel is provided with an inner well that contains an electrical heater and a Minco platinum resistance thermometer calibrated with reference to ITS-90. The adiabaticity is maintained by an inner copper adiabatic shield that is kept at the same temperature than the sample. An additional outer shield and a copper ring reduce the heat exchange through the wires and the instabilities in the temperature control. The data acquisition and the measuring conditions are computer controlled. The adiabatic conditions are maintained by a five-channel digital temperature controller interacting with the running program and acting on the signals of differential thermocouples referred to the sample temperature.

Measurements were taken by the step method, measuring the heat inputs and the temperature increments from 5 to 350 K. The molar heat capacity was calculated after subtracting the heat-capacity contribution of the empty sample holder measured on a separate experiment and has been represented in Fig. 3. A λ-type anomaly was observed with maximum at $T_0 = 158.1 \pm 0.3$ K. Typical temperature increments were 3 K, with smaller intervals below 30 K and around the transition temperature. The absolute accuracy of the calorimeter, obtained in calibrations with synthetic sapphire and OFHC copper, was 0.3%.

Heating and cooling thermograms were taken in the range 145–170 K by holding a constant temperature shift between the sample holder and the adiabatic shield, which produced an average heating or cooling rate of around 0.5 mK/s. Temperature and time were recorded every 20 s. To deduce the heat capacity by this technique, the rate of heat gain or loss is adjusted to a conduction and a radiation term that, for a constant temperature difference between sample and shield, is

$$\frac{dH}{dt} = \left(\frac{dH}{dT}\right)_p \frac{dT}{dt} = A + BT^3, \tag{1}$$

where H is enthalpy of sample plus holder, p pressure, and t time. The constants for the conduction and radiation terms,

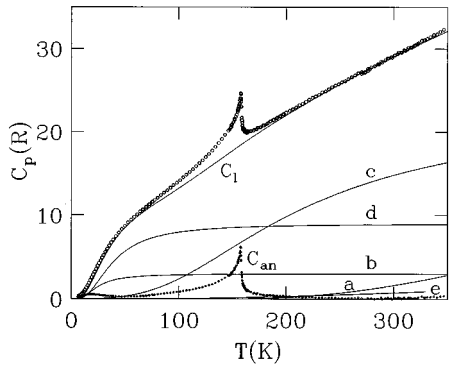

FIG. 3. Adiabatic heat-capacity data of $(CH_3)_4NBF_4$. The lattice contribution C_l has been obtained from the addition of the following components: (a) internal vibrations and rocking modes of CH_3 (five Einstein functions; see Table IV), (b) rotations of $(CH_3)_4N$ (one Einstein function with $T_E = 76$ K), (c) internal vibrations of BF_4 and C_4N plus torsional modes of CH_3 (22-dimensional Debye function with $T_{D1} = 880$ K), (d) translations and rotations of BF_4 and translations of $(CH_3)_4N$ (nine-dimensional Debye function with $T_{D2} = 160$ K), and (e) lattice expansion (Nernst-Lindemann approximation with $A = 3.6 \times 10^{-7}$ mol/J). The anomalous heat capacity C_{an} is the difference between the experimental points and C_l.

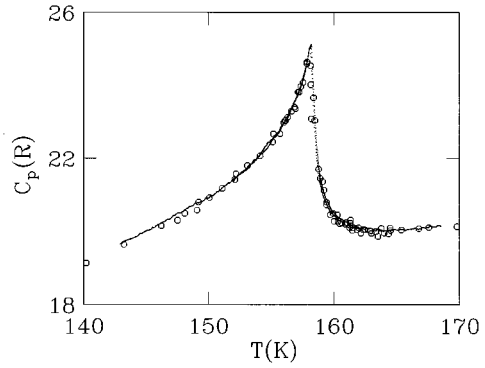

FIG. 4. Experimental heat-capacity points from the step measurements (○) and from the thermograms in the transition region.

A and B, are determined from the previously measured values $(dH/dT)_p = C_p$ at two temperatures T_1 and T_2 below and above the anomaly. The temperature drift dT/dt is deduced from the recording of T vs t, which allows us to have C_p as

$$C_p = \frac{A + BT^3}{(dT/dt)}. \tag{2}$$

To calculate A and B, the temperatures $T_1 = 150$ K and $T_2 = 162$ K were chosen. The value of (dT/dt) was obtained for every temperature by fitting a few points around each value of T with a straight line in the plot of T vs t. The number of points used for the fit varied with T in order to avoid an oversmoothing of the curve in the neighborhood of the peak. In this case 40 points (covering a range of 0.4 K) were taken below 157 K and above 159 K, gradually reducing this number down to 10 points near the peak. The resulting data of the molar heat capacity C_p, coalesced in both thermograms with the heat pulse points in the whole range, as it is shown in Fig. 4. A small difference of around 0.1 K found between the heating and the cooling curves is consistent with the dynamic rate and can be due to the absence of perfect thermal equilibrium. The C_p maximum appeared at 158.15 ± 0.05 K.

IV. ANALYSIS OF THE HEAT-CAPACITY DATA

A. Determination of the lattice contribution

The experimental molar heat capacity is a sum of the anomalous contribution C_{an} and the lattice part C_l. The latter one departs significantly from the usual shape in solids (i.e., Debye like) and shows a quite linear increase above the transition temperature. From an analysis of the structural features, the lattice part could be interpreted as the addition of the following contributions.

(a) Internal CH_3 vibrations, described by Einstein functions corresponding to normal modes of the molecule. The rocking modes of the CH_3 group have also been considered with an Einstein function. Since there are not direct measurements of their frequencies in this compound, the usual values found in the literature for methyl groups[13] have been used. The corresponding Einstein temperatures T_E and degeneracies g_i per molecule are listed in Table IV. Each mode contributes to the heat capacity with the expression

$$C_E = \frac{R g_i (T_E/T)^2 \exp(T_E/T)}{[\exp(T_E/T) - 1]^2}. \tag{3}$$

(b) Rotational motions of the $(CH_3)_4N$ groups. The exact rotational contribution to C_p for a tetrahedral top in an external potential is not a simple function. However, the rotational activation energy for jumps between different orientations have been deduced from proton-lattice relaxation time measurements,[4] obtaining $E_a/k_B = 2814$ K. As this value exceeds the temperatures of our interest in at least an order of magnitude, the molecular group experiences rotational oscillations of small amplitude (librations) and can be adequately described by a threefold degenerated Einstein function. The local symmetry of the $(CH_3)_4N$ is $\bar{4}$ but it does not differ very much from tetrahedral and has been treated like that for the sake of simplicity. For a tetrahedral molecule in a tetrahedral potential,[14] the harmonic approximation gives $\omega = \sqrt{9E_a/2I}$ (see the Appendix), I being the moment of in-

TABLE IV. Einstein temperatures and degeneracies of the vibrational and rocking modes of the CH_3 group.[a]

Mode	g_i	T_{Ei} (K)
Symmetric stretching	1	4132
Asymmetric stretching	2	4263
Symmetric bending	1	1984
Asymmetric bending	2	2100
Rocking	2	1636

[a]From Ref. 13.

ertia of the molecule. The value of I obtained from the structural data at RT gives the corresponding Einstein temperature $T_E=\hbar\omega/k_B = 76$ K.

(c) The internal vibrations of the molecular groups BF_4 and $(CH_3)_4N$ cannot be considered as local modes because of the strong interaction between them. Ignoring the hydrogen atoms, there are 18 degrees of freedom, plus the torsion of the 4 methyl groups around the C-N axis that makes a total of 22 degrees of freedom. So a 22-dimensional Debye function was used, with a heat-capacity contribution

$$C_{D1} = 66R\left(\frac{T}{T_{D1}}\right)^3 \int_0^{(T_{D1}/T)} \frac{(T_{D1}/T)^4 \exp(T_{D1}/T)\, d(T_{D1}/T)}{[\exp(T_{D1}/T)-1]^2}, \tag{4}$$

in which T_{D1} is the characteristic temperature.

(d) Translations and rotations of BF_4 and translations of $(CH_3)_4N$ can be described by a nine-dimensional Debye function, because they are collective motions of the lattice. These modes, of lower frequency than the previous ones, have been represented by a Debye contribution of characteristic temperature T_{D2}.

(e) The expansitivity of the lattice gives the difference between C_p and C_v. It has been calculated by the Nernst-Lindemann approximation

$$C_p - C_v = AC_p^2 T, \tag{5}$$

in which A is a fitted parameter.

The fitting parameters T_{D1}, T_{D2}, and A were chosen in order to reproduce the experimental heat capacity below 50 K and between 220 and 300 K. The following values were obtained: $T_{D1} = 880$ K, $T_{D2} = 160$ K, and $A = 3.6\times10^{-7}$ mol/J. Below 200 K, this last term is less than $0.24R$ (i.e., about 1% of the total C_p), not very significant indeed compared to the total lattice estimate.

A reasonable agreement between the calculated lattice contribution and the experimental values was obtained, except in the anomalous region. A small discrepancy found around 20 K is not significant for our study and is probably due to existence of van Hove singularities at low frequencies.

From 50 K to 250 K the difference between the measured C_p and the sum of these contributions, C_l, has been taken as the anomalous experimental heat capacity C_{an} and has been plotted in Fig. 3 together with each of these terms.

B. Analysis of the anomaly

The absence of thermal hysteresis suggests a second-order or weakly first-order transition. Therefore, the anomaly has been analyzed in the frame of Landau theory. The free energy Φ can be expanded in a power series of an order parameter η and written as[15]

$$\Phi - \Phi_0 = A_t(T-T_c)\eta^2 + B\eta^4 + C\eta^6 + \cdots, \tag{6}$$

in which A_t, T_c, B, and C are constants and $C>0$. The prediction for the heat capacity is obtained by minimization of Φ. If $B>0$, there is a second-order transition at a critical temperature T_c. If $B<0$, there is a first-order transition at a temperature T_0, and below this temperature

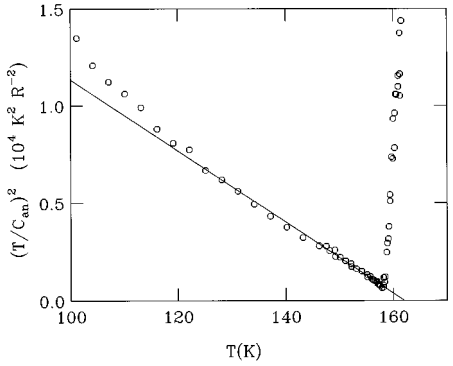

FIG. 5. Temperature dependence of the square reciprocal C_{an} as given in Eq. (7). The straight line represents the fit to Landau theory.

$$\left(\frac{T}{C_{an}}\right)^2 = \frac{4[B^2 - 3A_tC(T_0-T_c)]}{A_t^4} + \frac{12C(T_0-T)}{A_t^3}. \tag{7}$$

In a plot of $(T/C_{an})^2$ vs T, as shown in Fig. 5, one can observe that the experimental points fit well to a straight line below T_0. The extrapolation of $(T/C_{an})^2$ to 0 gives the tricritical temperature $T_{cr} = 162$ K (i.e., the temperature at which the transition would be of second order) and the slope, $-12C/A_t^3$ which gives $C/A_t^3 = 15.2\ \mathrm{J^{-2}\,mol^2\,K^3}$. From the previous relations one obtains

$$T_{cr} = T_c + \frac{B^2}{3A_tC}, \tag{8}$$

$$T_{cr} - T_c = 4(T_{cr} - T_0), \tag{9}$$

giving $B/A_t^2 = -\sqrt{12C(T_{cr}-T_0)/A_t^3} = -26.7\ \mathrm{J^{-1}\,mol\,K^2}$, and $T_c = 146.4$ K.

Above T_0, the fluctuations govern the value of C_{an}, which cannot be explained by classical Landau theory. A further development of the theory, including Gaussian fluctuations, gives C_{an} proportional to $(T-T_0)^{-0.5}$, though the influence of defects and impurities may not be negligible.[16] Moreover, fluctuations become more important in low-dimensional systems.

The critical behavior of the transition has been analyzed considering the measurements of the thermograms, in which reduced temperatures $t = T/T_0 - 1$ as small as 1.3×10^{-3} can be reached without rounding effects. A logarithmic plot of C_{an} vs t above the transition temperature shows a linear dependence with a critical exponent $\alpha = 0.50$ that coincides with the value predicted from fluctuation theory. Below T_0 and for a transition temperature close to the tricritical point, Landau theory predicts the same functional divergence. From the previous relations one obtains

$$\frac{C_{an}}{T} = \left(\frac{A^3}{12C}\right)^{1/2} (T_{cr}-T)^{-0.5}. \tag{10}$$

The experimental points, represented in a double logarithmic scale, are given in Fig. 6 together with a straight line with

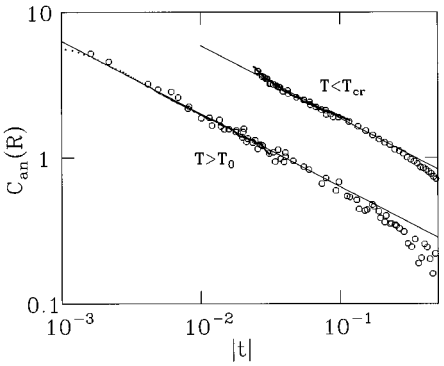

FIG. 6. Double logarithmic plot of C_{an} vs reduced temperature from the adiabatic and thermograms data. The straight lines correspond to a critical exponent $\alpha=0.50$ below and above the transition temperature, being $C_{an}\propto|t|^{-\alpha}$.

slope $-\alpha=-0.50$. This critical analysis can be done only down to a reduced temperature $|t| = |T/T_{cr}-1| = 2.5\times10^{-2}$, because of the difference between T_0 and T_{cr}.

The main conclusion of this analysis is that the transition, which looks like a second-order one at first sight, fits very well with Landau theory for a weakly first-order transition.

The anomalous entropy, obtained by integration of the peak from 50 to 250 K (avoiding the 0–50 K range where the lattice estimate is poor), gives $\Delta S/R=1.4\pm0.1$, very close to ln 4, which is another indirect test for the type of order-disorder transition described in the structural section. The anomalous entropy must be ln N, N being the ratio of multiplicities between the high- and the low-temperature orientations.

V. MONTE CARLO SIMULATION

A. Energy calculations

The BF_4 tetrahedra can be considered as forming two interpenetrating networks having one B-F bond in the c axis and oriented in opposite directions on each network. The different orientations of the two networks are forced by strong electrostatic constraints coming from the interaction with the rest of the lattice. In the RT symmetry there are four possible equivalent orientations of equilibrium for each BF_4 tetrahedron within each network, choosing one of them in an ordered way in the LT structure.

Each BF_4 tetrahedron is surrounded by four members of the opposite network on the ab plane, forming two interpenetrating square planar configurations. The two neighbors in the c axis belong to the same network. Due to the 4 possible orientations of each tetrahedron, there are 16 relative orientations for each pair of BF_4 groups.

The electrostatic interaction between the BF_4 groups is essentially octupolar. The interaction energies have been calculated for every orientation of the BF_4 nearest neighbors, considered as regular tetrahedra and taking the B-F distance from the RT structural data, $d=1.335$ Å.[5] Initially, each F^- ion has been considered as a point charge with $q_F=-1e$. The mass centers of the tetrahedra lie roughly on the ab plane, slightly shifted from $z=0$ by ±0.49 Å and separated from each other 5.9 Å. The distances between planes are 5.8 Å. Therefore, the BF_4 mass centers form a distorted simple cubic lattice. The octupole-octupole interaction energy is proportional to O^2/r^7, O being the octupolar moment of the molecular group and r the distance between the interacting groups. As a comparison, NH_4Cl orders at 242 K due to the octupolar interaction of the NH_4^+ ions, being the effective charge of H^+, $q_H = 0.18$ to $0.5e$, the N-H distance 1.05 Å, and the intermolecular distance 3.87 Å.[17] Considering the large value of the BF_4 octupolar moment and that their octupole-octupole distance in our compound is 1.5 times longer, one could expect that BF_4 would order at a temperature above 200 K. Using a smaller effective F^- charge, instead of $q_F=-1e$, would lower the transition toward the experimentally found value. In any case, the octupole-octupole interaction is very dependent on the relative orientation of the molecules and, in this case, is different than in NH_4Cl. Surprisingly, the interaction energies between the nearest BF_4 groups in adjacent layers differ only between 0 K and 22 K for the different relative orientations permitted by the rest of the lattice. On the other hand, the interaction energies between nearest groups lying on the same layer range from 0 to the strikingly large value of 6441 K. The interaction between next-nearest neighbors is much weaker because the r^{-7} dependence of the octupole-octupole interaction. Table V gives the energies for all the relative orientations of BF_4. Representative orientations for each one of the different energies are shown in Fig. 7.

By simple inspection of Fig. 7 and Table V, one can see the impossibility of orienting the BF_4 tetrahedra in such a way that all the nearest neighbors interact with energies E_0 or E_1. The minimum energy compatible with long-range or-

TABLE V. Electrostatic interaction energies for the different equilibrium orientations of two nearest BF_4 groups lying on the same ab plane. The positions a and b correspond to the BF_4 groups with the central B atom in sites $(\overline{x+1/2},x,\overline{z})$ and $(\overline{x},x+1/2,z)$; they are also shown in Fig. 7. The relative orientations for the other positions can be related by symmetry operations. There are six different energy values: $E_0=0$, $E_1=225.4$ K, $E_2=2821.5$ K, $E_3=3069.3$ K, $E_4=6164.4$ K, and $E_5=6441.2$ K. The lowest energy has been taken conventionally as zero.

a	b	E
1	1	E_3
1	2	E_2
1	3	E_4
1	4	E_5
2	1	E_2
2	2	E_3
2	3	E_5
2	4	E_4
3	1	E_0
3	2	E_1
3	3	E_3
3	4	E_2
4	1	E_1
4	2	E_0
4	3	E_2
4	4	E_3

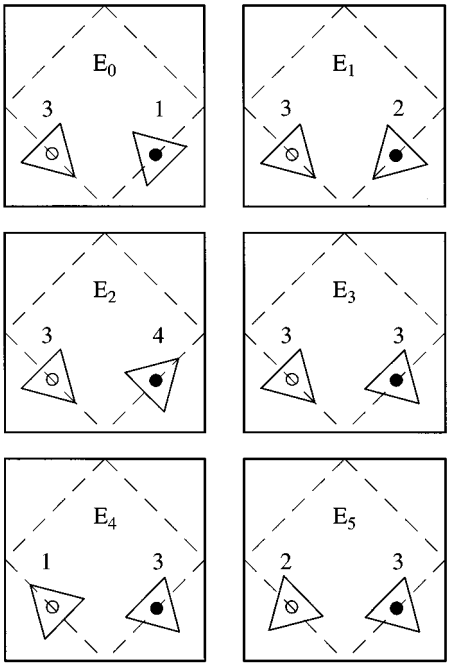

FIG. 7. Representative relative orientations of pairs of BF_4 nearest neighbors corresponding to the six different interaction energies, E_0–E_5, as listed in Table V.

der is E_2, much higher than E_0 or E_1. Then, the system is highly frustrated, which would explain the ordering at comparatively low temperature.

B. Computer simulations

A Monte Carlo simulation has been used to calculate the equilibrium configuration at each temperature and the thermodynamic functions, taking the next simplifying assumptions.

(a) Electrostatic interactions between nearest BF_4 neighbors in the same layer have only been considered. The indirect interactions, through polarization of the other atoms, have been neglected.

(b) Each BF_4 group has been considered as a rigid regular tetrahedron which can jump between four equilibrium orientations, with no other degrees of freedom.

(c) All the lattice deformations have been neglected.

A finite square lattice of 50 × 50 sites with periodic boundary constraints was simulated by a computer program. An importance sampling method was used with a Metropolis algorithm for thermalization, in which the transition probability to a new state is 1 for a lower-energy state and $\exp(-\Delta E/k_BT)$ for a higher-energy state, ΔE being the energy increment to the new state. This probability is compared to a random number between 0 and 1. When the transition probability is higher than the random number, the transition is permitted; otherwise, the system remains in the same state.

Starting either from the ordered configuration given by the LT structural results or from a completely disordered state, the evolution of the energy with the Monte Carlo time was monitored at different temperatures. One Monte Carlo step (MCS) has been defined as a complete sweep through the lattice. The sweep is made at a random order to avoid

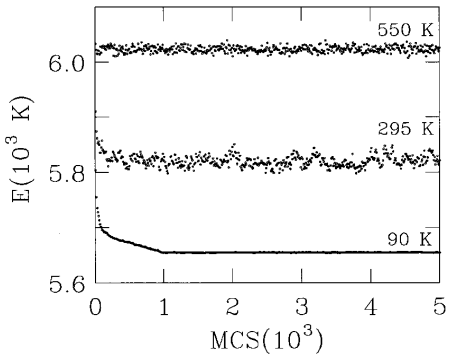

FIG. 8. Thermalization of the configurational energy of a 50×50 square lattice of BF_4 tetrahedra at 90 K, 295 K, and 550 K through 5000 MCS.

correlations, but passing once by every lattice point and trying one random orientation among the four possible choices. Thermal equilibrium was reach for less than 1000 MCS at every temperature checked. Therefore, 2000 MCS were permitted for thermalization at each temperature and 2000 additional configurations were used for the calculation of the average energy and the heat capacity, taken from the energy fluctuations

$$C=\frac{N}{k_BT^2}\sum_i (E_i^2-\overline{E^2}), \tag{11}$$

where E_i is the energy for each configuration and $\overline{E}$ the average value for the 2000 configurations. In the vicinity of the transition, 5000 configurations were taken for the calculation of the thermodynamic quantities, due to their increased dispersion.

Figure 8 shows the thermalization processes at three characteristic temperatures over 5000 MCS, starting from a completely disordered structure. One can observe the number of steps needed to reach thermal equilibrium and the different effect of low and high temperatures on the dispersion of the points. For the transition region an increase of the energy fluctuations is also observed. The stability of the equilibrium energies and the heat capacities has been followed, at these temperatures, over 50 000 MCS to be sure that the equilibrium has been reached.

For the temperature evolution, the previous equilibrium configuration has been taken as the starting configuration for each temperature. The equilibrium energy vs temperature has been represented in Fig. 9 and the corresponding heat capacity in Fig. 10. This evolution has been calculated on heating and on cooling, finding the same results without any hysteresis. Only if the system is quenched at a very low temperature from a disordered configuration a metastable configuration is obtained with slightly higher energy.

C. Analysis of the results

From the energy curve, one can see that the high-temperature configuration is a random distribution of the BF_4 tetrahedra in the four permitted orientations. The energy tends to the high-temperature limit, which is 2 times the average of the energies in Table V, because in a square lattice of N molecules there are $2N$ pairs of nearest neighbors.

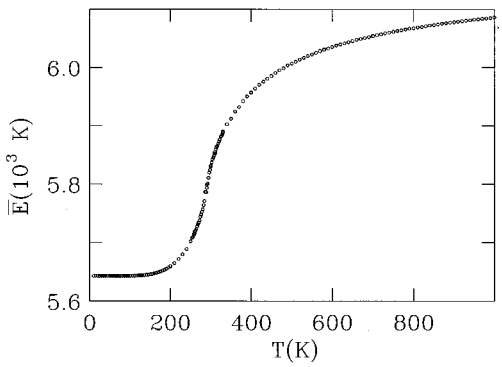

FIG. 9. Monte Carlo calculations for the temperature variation of the average energy in a 50×50 lattice of BF_4 tetrahedra.

For a random state, the average energy is $\overline{E}(T=\infty)=2(2E_0+2E_1+4E_2+4E_3+2E_4+2E_5)/16=6153.15$ K, as obtained in the simulation.

When the temperature is slowly lowered, $\overline{E}$ decreases monotonically down to 5643 K at the lowest temperature, which coincides with $2E_2$ of Table V. The ground state is described by the configuration experimentally found in the crystallographic section, as shown in Fig. 1.

The heat capacity is small at low and high temperatures, but reaches a sharp maximum at 290 ± 5 K. Similar calculations with smaller lattices give the same temperature for the peak.

Configuration domains obtained at four characteristic temperatures are shown in Fig. 11. The BF_4 groups belonging to the first domain type (white) are arranged as shown in Fig. 1 and correspondingly through the whole lattice. Rotating one of the BF_4 groups 90°, 180°, and 270° and arranging the rest of the lattice accordingly, one can obtain the orientation of the BF_4 group on each lattice site for the other domains (light grey, dark grey, and black). One of the domains prevails at low temperatures with nucleation of small domains of the other three types due to thermal excitation. Just at the temperature of the heat-capacity maximum, the low-temperature domain percolates over the whole lattice, with important cluster growth of the other domains. On passing above the temperature of the maximum, the long-range order disappears, maintaining a strong short-range order in large domains of ordered regions. The size of the domains

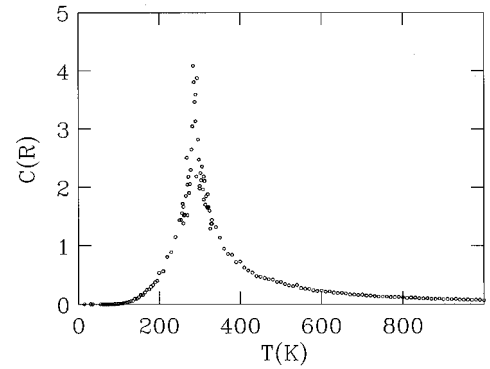

FIG. 10. Temperature dependence of the heat capacity calculated from the energy fluctuations in the Monte Carlo calculations.

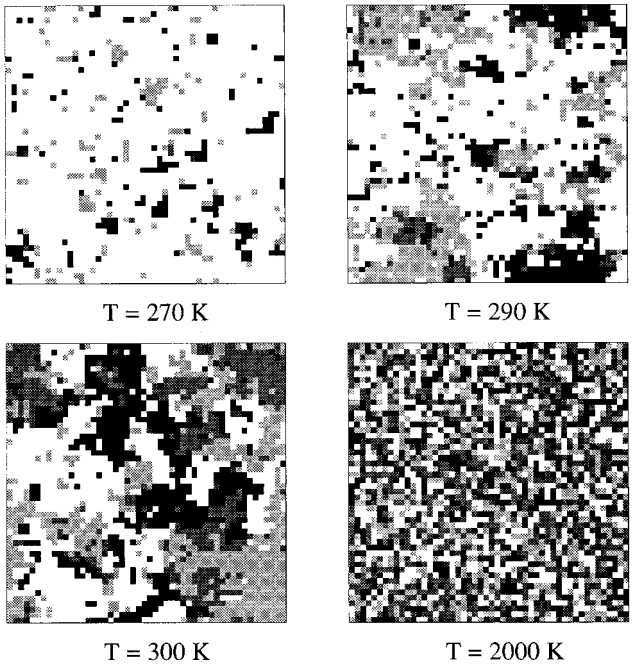

FIG. 11. Typical domain structure for the four type of domains (in white, light grey, dark grey, and black) described in Sec. V C. Four characteristic temperatures have been taken: below T_0 (270 K), at T_0 (290 K), slightly above T_0 (300 K), and at very high T (2000 K).

decreases rapidly on increasing the temperature, giving a random distribution of very small clusters.

Considering the evolution of the configuration domains, the heat-capacity peak of the simulation must be identified with the ordering temperature in the real system. It should be noted that if the F^- charge were $q_F=-0.74e$ (probably more realistic than the value used, $q_F=-1e$), the ordering temperature would be the experimentally found, $T_0=158$ K, because it is proportional to q_F^2.

VI. CONCLUSIONS

The results of the Monte Carlo simulations in two dimensions, based on the electrostatic interactions of the BF_4 tetrahedra, predict correctly the low- and high-temperature configurations found in the x-ray experiments. A phase transition is found at a temperature compatible with the value found experimentally from the calorimetric study. We can conclude that the electrostatic octupole-octupole interaction between the BF_4 molecules is the mechanism producing the order-disorder transition.

The structural transition is, nevertheless, three dimensional. The order in the third dimension is driven by smaller interactions in which both tetrahedral groups of the formula unit have to be considered. Qualitative considerations on the electrostatic interactions yield a parallel orientation of superimposed BF_4 tetrahedra, as found experimentally. The details of the heat-capacity anomaly shape and the critical exponents depend on all the interactions. One cannot expect a perfect correspondence between the experimental values and the Monte Carlo calculations.

The energy calculations have been performed with a sim-

plified model. The introduction of the interactions of the BF_4 tetrahedra with the surrounding $(CH_3)_4N$ groups, the polarizability of the ions, and the small distortions from the tetrahedral configurations would stabilize more strongly the low-temperature configuration. The consideration of the lattice contraction at low temperatures would also increase the stabilization energy of the low-temperature configuration.

The lattice contribution to the heat capacity has been explained from considerations of the normal modes, with only three adjustable parameters. The anomalous contribution has been deduced by subtraction of the lattice part. The calculated entropy content $R\ln 4$ agrees with the value expected from the different equilibrium positions found for the BF_4 group below and above the transition.

The heat-capacity anomaly is well described by mean-field Landau theory. It is a weakly first-order transition and the critical exponents adjust very well to the value expected at both sides of the transition temperature.

ACKNOWLEDGMENTS

We thank the assistance of Dr. F. Lahoz in the diffraction experiments. Financial support from the Spanish CICYT, Project No. MAT94-0804, and from the Spanish-Italian bilateral Integrated Action HI94-104 is greatly acknowledged.

APPENDIX: EINSTEIN TEMPERATURE CALCULATED FROM THE ACTIVATION ENERGY FOR JUMPS OF TETRAHEDRAL MOLECULES

The symmetry of an undistorted $(CH_3)_4N$ group is tetrahedral. Its site symmetry in the $P4/nmm$ phase of $(CH_3)_4NBF_4$ is $4m2$, but its nearest neighbors, labeled F1 in this paper, form a quasitetrahedral cage. In the simplest form, the potential can be written as

$$V(\phi,\theta,\psi)=\beta B V_3(\phi,\theta,\psi), \tag{A1}$$

(ϕ,θ,ψ) being the Euler angles describing the orientation of the tetrahedron, $V_3(\phi,\theta,\psi)$ the lowest-order nonconstant function invariant under the tetrahedral symmetry of the group and under the site symmetry in the lattice, $B=\hbar^2/(2I)$, I the moment of inertia of molecule, and β a negative dimensionless parameter. The activation energy for the librational movements of the group can be calculated as the energy in the saddle point between two minima minus the zero-point energy of the group librations. For high barriers and for the high value of I in $(CH_3)_4N$, the zero-point energy can be neglected because $B/k_B \approx 1$ K. The barriers for rotations around the twofold and around the threefold axes can be calculated with the parameters given in the Appendixes A and B of Ref. 14. The lowest-energy barrier for rotational jumps happens around the threefold axis of the molecule and is given by

$$E_a=\frac{8\sqrt{7}}{9}(-\beta B). \tag{A2}$$

The librational frequency is

$$\hbar\omega=7^{1/4}\sqrt{8|\beta|}B. \tag{A3}$$

Then, taking the activation energy $E_a=23.4$ kJ/mol given from NMR experiments,[4] the Einstein temperature for the librational modes is

$$T_E=\frac{\hbar}{k_B}\sqrt{\frac{9E_a}{2I}}=76\text{K}. \tag{A4}$$

[1] G. Zabinska, P. Ferloni, and M. Sanesi, Thermochim. Acta **122**, 87 (1987).
[2] S. Jurga, J. Depireux, and Z. Pajak, *Proceedings of the Congrese Ampère 18th* [Magn. Reson. Relat. Phenom. **2**, 403 (1975)].
[3] M. Mahajan and B. D. Nageswara Rao, J. Phys. C **7**, 995 (1974).
[4] S. Torre and P. Ferloni, Z. Naturforsch. Teil A **47**, 721 (1992).
[5] G. Giussepetti, F. Mazzi, C. Tadini, P. Ferloni, and S. Torre, Z. Kristallogr. **202**, 81 (1992).
[6] C. W. Garland, K. J. Lushington, and R. C. Leung, J. Chem. Phys. **71**, 3165 (1979).
[7] R. Burriel, C. Piqué, E. Palacios, J. Rubín, J. Bartolomé, A. Bulou, and J. L. Fourquet, Ferroelectrics **108**, 219 (1990).
[8] H. Yasuda, Prog. Theor. Phys. **45**, 1361 (1971).
[9] N. G. Zamkova and V. I. Zinenko, Sov. Phys. Solid State **34**, 1464 (1992).
[10] G. M. Sheldrik, computer code SHELX76, Cambridge University, Great Britain, 1976.
[11] See AIP Document No. E-PAPS file via: http://www.aip.org/epaps/epaps.html E-PRBMDO-54-9099-70 KB for the structure factor tables. There is no charge for retrieval of electronic PAPS document files from the FTP server. For further information: e-mail: paps@aip.org or fax: 516-576-2223.
[12] E. K. H. Salje, *Phase Transitions in Ferroelastic and Coelastic Crystals*, *Cambridge Topics in Mineral Physics and Chemistry* (Cambridge University Press, Cambridge, England, 1992).
[13] J. R. During and J. F. Sullivan, *Infrared and Raman Spectra*, *Physical Methods of Chemistry* (John Wiley and Sons, New York, 1987), Vol. IIIA.
[14] D. Smith, J. Chem. Phys. **86**, 4046 (1987).
[15] K. S. Aleksandrov and I. N. Flerov, Sov. Phys. Solid State **21**, 195 (1979).
[16] A. P. Levanyuk, V. V. Osipov, A. S. Sigov, and A. A. Sobyanin, Sov. Phys. JETP **49**, 176 (1979).
[17] D. Smith, J. Chem. Phys. **82**, 5133 (1985).